Crystal Structure Determination of Cholesterol Oxidase from *Streptomyces* and Structural Characterization of Key Active Site Mutants[†,‡]

Q. Kimberley Yue,[§] Ignatius J. Kass,[||] Nicole S. Sampson,[||] and Alice Vrielink*[,§]

Biochemistry Department, McIntyre Medical Sciences Building, McGill University, 3655 Drummond Street, Montréal, Québec H3G 1Y6, Canada, and Department of Chemistry, State University of New York, Stony Brook, New York 11794-3400

Received October 20, 1998; Revised Manuscript Received December 29, 1998

ABSTRACT: Cholesterol oxidase is a monomeric flavoenzyme which catalyzes the oxidation and isomerization of cholesterol to cholest-4-en-3-one. The enzyme interacts with lipid bilayers in order to bind its steroid substrate. The X-ray structure of the enzyme from *Brevibacterium sterolicum* revealed two loops, comprising residues 78−87 and residues 433−436, which act as a lid over the active site and facilitate binding of the substrate [Vrielink et al. (1991) *J. Mol. Biol. 219*, 533−554; Li et al. (1993) *Biochemistry 32*, 11507−11515]. It was postulated that these loops must open, forming a hydrophobic channel between the membrane and the active site of the protein and thus sequestering the cholesterol substrate from the aqueous environment. Here we describe the three-dimensional structure of the homologous enzyme from *Streptomyces* refined to 1.5 Å resolution. Structural comparisons to the enzyme from *B. sterolicum* reveal significant conformational differences in these loop regions; in particular, a region of the loop comprising residues 78−87 adopts a small amphipathic helical turn with hydrophobic residues directed toward the active site cavity and hydrophilic residues directed toward the external surface of the molecule. It seems reasonable that this increased rigidity reduces the entropy loss that occurs upon binding substrate. Consequently, the *Streptomyces* enzyme is a more efficient catalyst. In addition, we have determined the structures of three active site mutants which have significantly reduced activity for either the oxidation (His447Asn and His447Gln) or the isomerization (Glu361Gln). Our structural and kinetic data indicate that His447 and Glu361 act as general base catalysts in association with conserved water H_2O541 and Asn485. The His447, Glu361, H_2O541, and Asn485 hydrogen bond network is conserved among other oxidoreductases. This catalytic tetrad appears to be a structural motif that occurs in flavoenzymes that catalyze the oxidation of unactivated alcohols.

Cholesterol oxidase (EC 1.1.3.6) catalyzes the oxidation of steroids containing a 3β-hydroxyl group and the isomerization of the Δ^5 double bond into conjugation with the ketone to form Δ^4-3-ketosteroids (Figure 1). The enzyme is secreted by a number of microorganisms that are capable of utilizing cholesterol as their sole source of carbon and energy. It is extensively used in clinical assays for the determination of serum cholesterol concentration in the diagnosis of arteriosclerosis and other lipid disorders. In addition, cholesterol oxidase has been used as a probe of membrane structure and cholesterol content (*3*). More recently, it has been found that cholesterol oxidase may act as a potent insecticidal agent, active against boll weevil larvae and other insects (*4*−*6*). The enzyme acts by lysing the cells of the mid-gut epithelium resulting in larval death. This lytic observation is explained by the fact that epithelial cell membranes are rich in 3β-hydroxy steroids. Upon ingestion of cholesterol oxidase, these steroids are converted to conjugated Δ^4-3-ketosteroids, and as a result, membrane leakage and subsequent cell lysis occurs. These findings suggest that cholesterol oxidase may be used as an agricultural pest control agent. A detailed understanding of its catalytic mechanism may provide important information for its optimization as an insecticidal agent (*7*).

In most cases reported to date, the monomeric enzyme contains one molecule of the prosthetic group flavin adenine dinucleotide (FAD)[1] tightly bound to each molecule of protein (*8*, *9*). A number of species have been reported to lack the FAD group (*10*−*12*). In addition, a second form of the enzyme has been identified in *Brevibacterium sterolicum* which contains the FAD cofactor covalently bound to a histidine residue of the protein via the 8-methyl group of the isoalloxazine ring system (*13*). Interestingly, the covalent

[†] This work is financially supported by the Medical Research Council of Canada (Grant MT-13341 to A.V. and a scholarship award to Q.K.Y.), the Fonds de la Recherche en Santé du Québec (Chercheur-boursier Salary Support Award to A.V.), the National Institutes of Health (Grant HL-53306 to N.S.S.), the Dreyfus Foundation (New Faculty Award to N.S.S.), the American Heart Association (Grant 94007160 to N.S.S.), and the U.S. Department of Education (GAANN fellowship to I.J.K.).

[‡] The coordinates for the native structure and the mutants have been deposited with the Brookhaven Protein Data Bank under Accession Numbers 14bv (native), 1cbo (His447Asn), 1cc2 (His447Gln), and 18bs (Glu361Gln).

* To whom correspondence should be addressed. Phone: (514) 496-6129. Fax: (514) 496-5143. E-mail: alice.vrielink@bri.nrc.ca.

[§] McGill University.

[||] State University of New York.

[1] Abbreviation: FAD, flavin adenine dinucleotide.

10.1021/bi982497j CCC: $18.00
Published on Web 03/17/1999

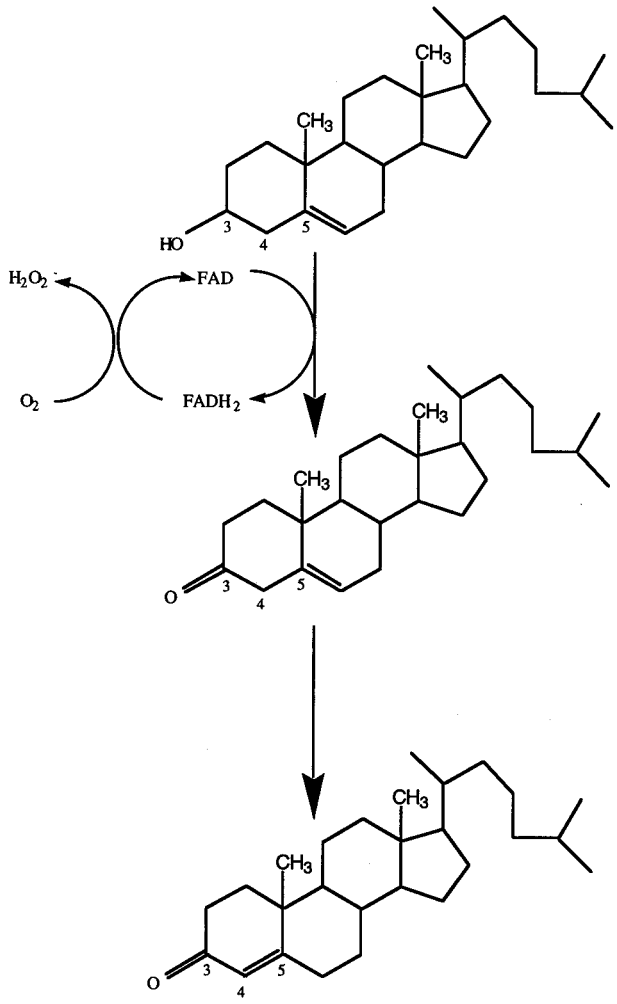

FIGURE 1: Reaction scheme of cholesterol oxidase using cholesterol as the substrate. The enzyme is bifunctional, catalyzing an oxidation and an isomerization reaction. The reduced flavin cofactor is reoxidized with molecular oxygen.

and noncovalent forms of the enzyme differ significantly in their redox potentials, suggesting a different protein environment around the flavin cofactor and particularly around the isoalloxazine ring system.

The crystal structure of cholesterol oxidase from *B. sterolicum* has been reported in both the presence and absence of a steroid ligand (*1*, *2*). These structures reveal a deeply buried active site which, in the absence of a steroid ligand, is occupied by a lattice of well-ordered water molecules. Two loop regions in the structure (residues 78−87 and residues 433−436) have poorly defined electron density, and the conformation of one of these loop regions (78−87) differs significantly between the steroid-free and steroid-bound structures. It was proposed that this loop region is important for interaction with the lipid bilayer in order to bind the steroid substrate. Sampson and co-workers have carried out studies to determine the degree of membrane disruption caused by cholesterol oxidase (*7*). These studies suggest that the enzyme interacts more with the phopholipid headgroups and less with the lipid regions of the fatty acids in the bilayer.

The crystallographic model of the enzyme has led to the suggestion of key amino acid residues important in the oxidation and in the isomerization mechanisms of the enzyme. Residue 447, a histidine, could act as the general base catalyst for abstraction of a proton from the C3-hydroxyl group of the steroid substrate during oxidation and, subsequently, as the general acid for stabilization of the dienolic intermediate of isomerization.[2] Residue 361, a glutamate, could act as the base that deprotonates the 4β-proton of the cholest-5-en-3-one intermediate. An alignment of the *Brevibacterium* and the *Streptomyces* cholesterol oxidase primary amino acid sequences shows that these residues are conserved (*14*). Their conservation supports their identification as important active site residues.

The structure of the *Brevibacterium* protein in the presence of a steroid ligand, dehydroisoandrosterone (*2*), revealed that, of the 13 bound water molecules, 12 were displaced by the steroid substrate. A single water molecule (H_2O541) remained, which forms hydrogen bonds with His447 and the C3-hydroxyl group of the substrate. These structural studies led us to suggest that general base catalysis by the histidine side chain is mediated through H_2O541, the remaining bound water molecule. Kinetic analysis of mutations in the *Streptomyces* cholesterol oxidase in which His447 is mutated to either an asparagine or a glutamine has shown that the imidazole is required for efficient catalysis of oxidation, but not for catalysis of isomerization (*15*). Thus, a base is required for removal of the hydrogen on O3 and efficient oxidation to the ketone. However, a general acid imidazolium ion is not required for formation of the dienolic intermediate of isomerization. A hydrogen bond network between an amide and O3 mediated by a water is sufficient, and catalytic rates equal to wild type are observed.

In the structure of the enzyme from *Brevibacterium* complexed with a steroid ligand, Glu361 is positioned over the β-face of the steroid in close proximity to the 4β-proton. The diffuse electron density and high temperature factors for this glutamate side chain indicate that it is a mobile residue. This mobility facilitates the proposed role for Glu361 as both a base involved in proton abstraction at C4 of the steroid A ring and as a conjugate acid in protonation at the steroid C6 position. Indeed, mutagenesis of this residue in the *Streptomyces* cholesterol oxidase to a glutamine resulted in complete suppression of the isomerization reaction; however, the oxidation reaction still occurred (*16*). Thus the product of the E361Q reaction is cholest-5-en-3-one, and it is produced catalytically. That is, the mutant enzyme releases the intermediate of the wild-type reaction and is capable of multiple turnovers.

To correlate fully the kinetic data with structure, we have carried out a crystallographic analysis of cholesterol oxidase from *Streptomyces* in the native form and the three mutants described above. These structures confirm the conservation of His447 and Glu361 between *Brevibacterium* and *Streptomyces*. Furthermore, they highlight the importance of the water organization in the active site for efficient catalysis. In particular, H_2O541 acts as the keystone for the active site. It forms a network of hydrogen bonds between the active site residues His447, Glu361, and Asn485.

In addition, these studies enabled us to identify structural differences between the *Brevibacterium* and the *Streptomyces* enzymes that rationalize the differences in activity between

[2] His447 is encoded by codon 484 in the *Streptomyces* gene (*24*) and codon 492 in the *Brevibacterium* gene (*14*); Glu361 is encoded by codons 398 and 406, respectively.

Table 1: Data Collection and Processing Statistics

data set	temperature (K)	resolution (Å)	total reflections	independent reflections	completeness (%)	I/σ	R_{merge} (%)
native	115	1.5	402 969	62 747	87.4	27.5	4.5
E361Q	115	1.65	281 106	49 835	91.8	35.1	5.0
H447N	293	1.8	150 280	38 759	90.0	24.6	5.4
H447Q	293	2.2	43 413	22 463	95.0	8.9	7.2

the two enzymes that have been observed (*17*, *18*). Furthermore, these differences, in combination with previous work characterizing a loop deletion mutant (*18*), suggest the structural origins of substrate specificity. This structural information will be useful in the future design of cholesterol oxidases with altered substrate activities and specificities.

EXPERIMENTAL PROCEDURES

Crystallization Conditions. Cholesterol oxidase from *Streptomyces* was mutagenized, expressed, and purified as described by Kass and Sampson (*15*). Crystals were grown by vapor diffusion using the hanging drop method. The precipitant conditions are 10−12% (w/v) poly(ethylene glycol) (PEG) MW 8000, 100 mM sodium cacodylate, pH 5.2, and 75 mM $MnSO_4$. Equal volumes of the protein (at a concentration of 8.5 mg/mL in 10 mM Hepes buffer, pH 7.0) and the precipitant were mixed in a drop and equilibrated against a well containing the precipitant at 17 °C. Single crystals appeared; however, they were too small for diffraction. Streak seeding techniques were applied (*19*), resulting in single usable crystals within 2−3 days. The typical crystal size was 0.2 × 0.1 × 0.1 mm. The crystals diffract to better than 1.0 Å resolution at synchrotron radiation beamline X8-C (Brookhaven National Laboratories). The reflections could be indexed on a monoclinic lattice corresponding to space group $P2_1$ with unit cell dimensions $a = 51.3$ Å, $b = 73.0$ Å, $c = 63.0$ Å, and $\beta = 105.1°$. Assuming one molecule per asymmetric unit, the V_m value is 2.2 Å^3/Da with a solvent content of 44%.

Crystals for both of the three mutant forms of the enzyme (E361Q, H447N, and H447Q) were obtained by introducing nucleation sites through streak seeding using crystals of the wild-type enzyme. The small single crystals which appeared were then used for macroseeding. Several small crystals were washed in 16% (w/v) PEG MW 8000 mother liquor three to four times and transferred to hanging drops which were preequilibrated against the original crystallization mother liquor. The space group and unit cell dimensions for the mutant crystals were identical to those of the native enzyme.

Data Collection and Processing. Data collection was carried out on native crystals at 115 K in order to minimize crystal decay. The crystals were transferred briefly to a cryoprotectant solution containing 12% glycerol in the crystal mother liquor. From this solution, a single crystal was mounted in a cryoloop (Hampton Research, Laguna Hills, CA) and placed in a cold nitrogen stream at 115 K (Oxford Cryosystems, Oxford, U.K.). The data were collected using Cu Kα radiation from a Rigaku RU-300 rotating-anode source and an RAXIS IIC image plate detector. A complete data set to 1.5 Å resolution was collected using a single crystal.

Data for the E361Q mutant crystals were also collected at low temperature; however, 20% ethylene glycol (v/v) in the crystal mother liquor was used as the cryoprotectant solution. Data collection to 1.65 Å resolution was carried out using a single crystal.

Both the H447N and H447Q mutant crystals were sensitive to various cryoprotectant solutions; therefore, room temperature data collection was carried out. For the H447N mutant data to 1.8 Å resolution were collected from two crystals and merged together. In the case of the H447Q mutant, data from a single crystal were collected to 2.2 Å resolution.

All images were processed with DENZO and the reflections merged and scaled with SCALEPACK (*20*). The details of the data collection and processing are presented in Table 1.

Structure Solution and Refinement. The crystal structure was solved by molecular replacement techniques. The program AMoRe (*21*) was used to obtain a structure solution for cholesterol oxidase from *Streptomyces*. The search model used was cholesterol oxidase from *B. sterolicum*, the structure of which has been refined to 1.8 Å resolution. Sequence comparison of the two forms of the enzyme reveals an amino acid identity of 58%. The search model was constructed as follows: amino acid residues which were identical in the two enzymes were maintained, and residues which were not identical were truncated to alanine. In addition, the FAD cofactor was eliminated from the search model. The search model was placed in an orthogonal cell, with dimensions four times the size of the minimal molecular dimensions. It was positioned in the cell such that the center of gravity was at the origin and the principal axes of inertia were parallel to the orthogonal axes. A rotation function was calculated using data from 20 to 2.5 Å resolution. Two solutions with peak heights of 23.6σ were found, where σ is the standard deviation of the rotation function. The translation function was calculated in the resolution range from 8.0 to 2.5 Å. For each rotational solution the translation function yielded a solution with a peak height of 23.3σ (σ is the standard deviation of the translation function), a correlation coefficient of 48.8, and an *R*-factor of 45.8%. The appropriately oriented model was subjected to rigid body refinement using data in the resolution range from 20 to 2.5 Å. The final solution had a correlation coefficient of 57.6 and an *R*-factor of 44.8%.

Model Building and Structure Refinement. All model building procedures were carried out on a Silicon Graphics computer using the program O (*22*). Residue addition and correction took place in each rebuild process using Fourier maps calculated with coefficients $2F_o - F_c$ and $F_o - F_c$. Structure refinement was performed using the program X-PLOR version 3.843 (*23*). The free *R*-factor was monitored during the course of the refinement using a subset of 10% of the data randomly chosen from the total diffraction data. For the native structure the refinement was initially carried out using data in the resolution range 10−2.5 Å. The

Table 2: Crystallographic Refinement Statistics

data set	resolution range (Å)	no. of protein atoms	no. of water molecules	independent reflections	*R*-factor	free *R*-factor
native	20.0−1.5	3830	664	62 692	18.1	20.0
E361Q	20.0−1.65	3845	470	44 368	19.0	23.1
H447N	20.0−1.8	3841	295	38 716	15.9	19.4
H447Q	6.0−2.2	3829	507	21 309	14.7	23.5

Table 3: Deviations from Ideal Geometry

data set	rms bond lengths (Å)	rms bond angles (deg)	rms dihedrals (deg)	average main chain *B*-factors (Å^2)	average side chain *B*-factors (Å^2)
native	0.01	1.3	25.0	13.13	11.35
E361Q	0.01	1.4	24.9	12.43	12.50
H447N	0.01	1.3	25.0	21.50	22.43
H447Q	0.01	1.3	25.1	24.37	21.61

resulting maps were inspected, and five regions of the structure which appeared to be poorly modeled were deleted. These regions corresponded to residues 4−10, 76−80, 356−357, 394−395, and 436−437. Refinement, after deletion of these regions, was carried out using data in the resolution range 6−2.2 Å. Manual rebuild was carried out and the full model included with the exception of residues 1−3 and 436−437. At this point crystallographic refinement was extended to 1.8 Å resolution, and individual temperature factor refinement was included. A further nine rounds of refinement and rebuilds were performed using data in the resolution range 6.0−1.5 Å with 2.0σ cutoff. The final round of refinement included all data from 6.0 to 1.5 Å with no σ cutoff and with no constraints to the FAD cofactor. Bulk solvent corrections were included at the final stages of the refinement using data from 20 to 1.5 Å. The final model for the native structure includes 498 amino acid residues of which 11 residues have been modeled with alternate conformations and 53 non-hydrogen FAD atoms. In addition, 664 water molecules have been included into the model. Only water molecules which make hydrogen-bonding contacts with the protein, FAD, or other water molecules and which have *B*-factors less than 50 Å^2 were included in the model. Table 2 shows the final refinement statistics for the native structure. Table 3 gives the final deviations of the model from ideal geometry.

Refinements of the mutants were essentially identical to the procedures used for the native protein. The initial electron density maps were calculated in X-PLOR using 90% of the reflection data in the resolution range from 15 to 1.8 Å for the H447N mutant structure, 15 to 1.65 Å for the E361Q mutant structure, and 15 to 2.2 Å for the H447Q structure. The side chains of the mutated residues were truncated to alanine in the first round of refinement, and the water molecules located in the active site were removed. The difference density maps clearly showed the mutated side chains enabling the mutation to be incorporated into the structural model. A total of seven rounds of refinement were carried out for the H447N mutant structure in the resolution range from 6.0 to 1.8 Å. For the H447Q mutant six rounds of refinement were carried out in the resolution range from 6.0 to 2.2 Å, and for the E363A mutant five rounds of refinement were carried out using data in the resolution range from 6.0 to 1.8 Å. The final refinement statistics are given in Table 2. The coordinates for the native structure and the three mutants have been deposited in the Protein Data Bank.

RESULTS AND DISCUSSION

Native Structure. The amino acid sequence identity between the enzyme from *B. sterolicum* and that from *Streptomyces* is 58%. For ease of comparison, the numbering of the *Streptomyces* structure is identical to that used for the *Brevibacterium* structure. Key residues which are located in the active site and which are involved in cofactor binding are completely conserved between the two enzymes. As expected, therefore, the native structure of the enzyme from *Streptomyces* was essentially identical to that of cholesterol oxidase from *Brevibacterium*. The structure consists of two domains, an FAD-binding domain, comprising a central mixed β-pleated sheet sandwiched between α-helices, and a steroid-binding domain made up predominantly of a large β-pleated sheet (see Figure 2). A large active site cavity is located between these two domains, buried well within the molecule and sequestered from the external aqueous environment of the protein, yet filled with a well-ordered lattice of water molecules.

Active Site Residues and Water. The substrate-binding site of the *Streptomyces* enzyme contains a lattice of water molecules analogous to what has been observed in the *Brevibacterium* enzyme. However, 14 water molecules are observed in the *Streptomyces* cavity as compared to 13 in the *Brevibacterium* enzyme structure (Figure 3). The seven water molecules positioned at the base of the active site closest to the flavin ring system are superimposable between the two structures. However, the more distal water molecules positioned nearer to the entrance to the binding site differ considerably in their position in the two structures. Further significant differences in the water structure are discussed in the sections on the mutant structures.

FAD Cofactor. The FAD cofactor adopts a conformation identical to that observed in the structure of the enzyme from *Brevibacterium*. The residues which make contact with the FAD cofactor are completely conserved in the two forms of the enzyme and make identical contacts to the cofactor. In fact, even the water molecules that contact the cofactor are conserved in the two structures. In addition, an identical bending of the isoalloxazine ring system is observed between the cofactors of the two structures. The conservation of the FAD conformations is consistent with their UV spectra. The UV spectra of the *Streptomyces* and *Brevibacterium* bound FAD cofactors have nearly identical λ_{max}'s at 391 and 468 nm and at 388 and 469 nm, respectively (*18*, *17*).

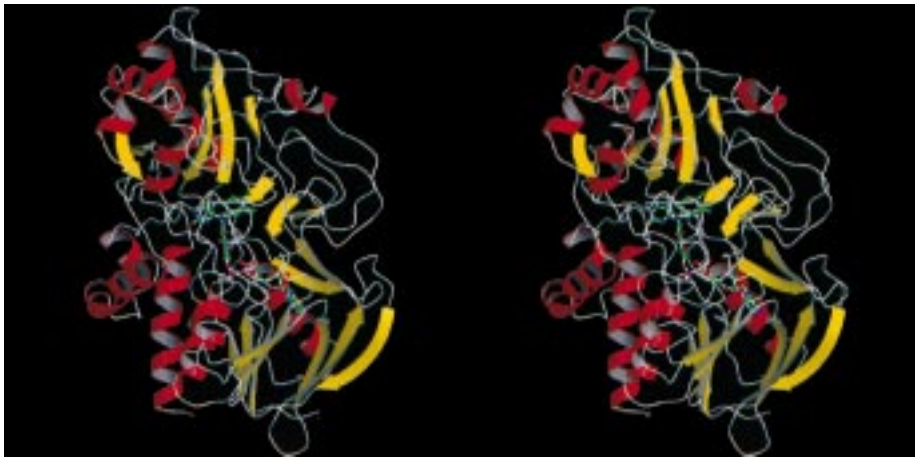

FIGURE 2: Stereo figure of cholesterol oxidase from *Streptomyces* showing the secondary structure elements. The α-helices are shown in red and the *β*-strands are shown in yellow. The FAD cofactor is displayed with a ball-and-stick representation. The figure was prepared with MOLSCRIPT (*32*) and RASTER3D (*33*).

FIGURE 3: Stereo figure of the active site region of cholesterol oxidase from *Streptomyces* showing the lattice of water molecules. The FAD cofactor is shown in thickened lines and residues lining the active site cavity are shown in thin lines. The water molecules are represented as spheres. The key residues implicated in substrate binding and catalysis and the water molecule remaining upon substrate binding have been labeled.

Substrate-Binding Site Loops. Comparison of the structures from *Streptomyces* and *Brevibacterium* shows that only one region of the structures differs significantly. The enzyme contains two loop regions that have been proposed to act as the entrance to the active site and make up a lid that covers the active site. These loop regions consist of residues 78−87 and 433−436. In the *Brevibacterium* structure the extended loop between residues 78 and 87 displays poor electron density and correlatively high atomic temperature factors. The steroid-bound form of the *Brevibacterium* enzyme also reveals poor electron density and high atomic temperature factors for this loop region, particularly on the solvent-exposed side of the molecule. The second loop region between residues 433 and 436 also has very poor electron density. Indeed, residues 434 and 435 could not be modeled as there was no significant density present. These observations indicated that these two loop regions were likely to be very flexible and led us to postulate that these regions composed the entrance to the active site pocket. In the structure from *Streptomyces*, these two loop regions are more highly ordered. The loop between residues 78 and 87 adopts a helical turn considerably different from the extended structure seen in the *Brevibacterium* structure (see Figure 4). The average temperature factors of all atoms within this region are 11.5 Å^2 as compared to 18.4 Å^2 in the *B. sterolicum* structure (the average temperature factors for all protein atoms in both structures are 10.3 Å^2 despite the fact that high-resolution data for the *B. sterolicum* structure were collected at 263 K and those for the *Streptomyces* structure were collected at 100 K). The second loop region between residues 433 and 436 is well ordered in the *Streptomyces* structure, whereas in the *Brevibacterium* structure, there was no electron density present in the map for residues 434 and 435. Inspection of crystal contacts revealed that these two loop regions are not involved in crystal contacts with neighboring molecules.

The loops in cholesterol oxidase are amphipathic in nature. Hydrophobic residues are directed toward the internal region of the molecule and the active site cavity, whereas the more hydrophilic residues are located on the external surface of the molecule. This amphipathic nature is maintained in the structure of the *Streptomyces* enzyme despite the fact that the chain adopts an alternative conformation to that seen in the *Brevibacterium* enzyme. The appearance of these loop regions making up the entrance to the active site of the enzyme is reminiscent of the pancreatic and fungal lipase structures in which the entrance is also made up of relatively mobile α-helix and loop regions (*25*−*27*). In both cholesterol

FIGURE 4: Stereo figure showing the superposition of the loop region between residues 78 and 97 in the structures of cholesterol oxidase from *Brevibacterium* and *Streptomyces*. The darker shaded molecule represents the loop region in the structure from *Streptomyces*, and the lighter shaded ribbon represents the loop region in the structure from *Brevibacterium*.

Table 4: Michaelis−Menten Rate Constants for *Streptomyces* and *Brevibacterium* Wild-Type Cholesterol Oxidase

	cholesterol[a]			dehydroepiandrosterone[b]		
	k_{cat} (s^{-1})	K_m (μM)	k_{cat}/K_m (M^{-1} s^{-1})	k_{cat} (s^{-1})	K_m (μM)	k_{cat}/K_m (M^{-1} s^{-1})
Streptomyces (*15*, *17*)	44 ± 2	3 ± 0.4	1.5×10^7	0.69 ± 0.01	27.5 ± 0.5	2.5×10^4
Brevibacterium (*18*)	nd[c]	>100	$5.0\ (\pm 0.2) \times 10^5$	4.8 ± 1	400 ± 100	1.2×10^4

[a] Assays were conducted in 50 mM sodium phosphate, pH 7.0, 0.025% Triton X-100, and 2% propan-2-ol at 37 °C. [b] Assays were conducted in 50 mM sodium pshophate, pH 7.0, and 10% EtOH at 37 °C. [c] nd, not determined.

oxidase and lipase, the amphipathic lids cover the substrate-binding sites to prevent aggregation of the proteins at their hydrophobic sites. The similarities of substrate hydrophobicities and their lid architectures support the hypothesis that the hydrophobicity of the substrate dictates the molecular architecture for substrate binding (*28*).

Relationship of Wild-Type Activity to Native Structure. Despite the 58% amino acid sequence identity between *Brevibacterium* and *Streptomyces* cholesterol oxidases, their catalytic activities are different (Table 4). With Triton X-100 solubilized cholesterol as substrate, the specificity constant k_{cat}/K_m is 50-fold higher for the *Streptomyces* oxidase. This difference in activity is due to the differences in K_m's. The K_m for the *Streptomyces* oxidase is 3 μM (*15*); the K_m for the *Brevibacterium* oxidase is greater than 100 μM, although it is not directly measurable due to the limited solubility of cholesterol (*17*). Both enzymes will also oxidize and isomerize the soluble substrate dehydroepiandrosterone. The k_{cat}/K_m's are reduced compared to cholesterol. Although the specificities of the two species for dehydroepiandrosterone are similar, the K_m of the *Brevibacterium* oxidase is higher than the *Streptomyces*. It should also be noted that the *Streptomyces* enzyme is 600-fold more specific for cholesterol than dehydroepiandrosterone, in contrast to the *Brevibacterium* enzyme that is only 25-fold more specific for cholesterol.

Comparison of the native *Streptomyces* and *Brevibacterium* cholesterol oxidase structures identifies the structural reasons for these differences. As described above, the active site residues are identical amino acids in identical positions. Moreover, the hydrogen-bonding network built around H_2O541 from the two native structures is superimposable. The FAD cofactors in both structures have identical contacts. It seems reasonable that the difference in activities between the two species does not arise from differences in the catalytic groups in the active site. The major difference between the two native structures is the structure of loop 78−87 and the thermal mobility of loop 433−436. These differences appear to translate into differences in substrate activity and specificity.

The higher temperature factors of the *Brevibacterium* loops in comparison to the *Streptomyces* loops correlate with the elevated K_m's and reduced specificity constants for cholesterol and dehydroepiandrosterone observed with the *Brevibacterium* enzyme. This correlation suggests that the increased catalytic efficiency of the *Streptomyces* enzyme is a result of the decreased flexibility of the loops. By orienting the residues that bind the tail of the steroid prior to binding, the entropy loss encountered during the catalytic steps is minimized, and the reaction rates are maximized.

Previously, we established that residues 79−83 of the *Streptomyces* enzyme determine substrate specificity for steroids substituted at C17 (*18*). It is these same residues that are in dramatically different conformations in the *Streptomyces* and *Brevibacterium* native structures. A structure with cholesterol, or another steroid containing the 8-carbon isoprenoid tail, bound in the active site would give the most insight into substrate specificity. Unfortunately, the limited solubility of cholesterol has hampered, thus far, crystallization of this complex. Nevertheless, the correlation between structural differences and activity differences corroborates our previous conclusions (*18*) about specificity based solely on kinetic observations. These structures suggest that changing the specificity of the enzyme to accommodate different C17 substituents will require more than changing the amino acids so that they complement the different C17 tails. If altered specificity is to be obtained without decreased catalytic efficiency, additional flexibility must not be introduced into the loop.

Structure of Glu361Gln. In the native structure, the glutamate-361 side chain is well ordered, and there is clear electron density for the entire side chain. This order is in contrast to what has been observed for the glutamate side chain in the structure of the *Brevibacterium* enzyme. In both the native structure (*1*) and the steroid complex structure (*2*) very poor electron density was observed for the glutamate

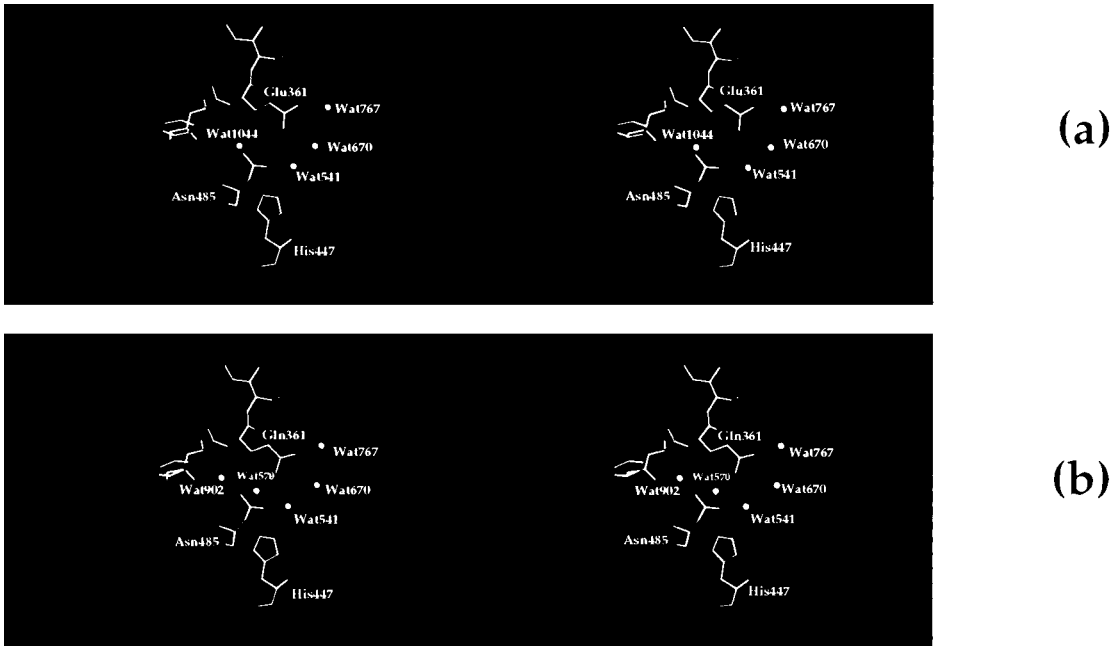

FIGURE 5: Stereo figures showing the water structure around residue 361 in the *Streptomyces* enzyme (a) native structure and (b) Glu361Gln mutant structure. The spheres represent water molecules, and the dashed lines correspond to hydrogen-bonding interactions.

side chain. Interestingly, despite the significant difference in electron density of the glutamate side chain between the structures of the *Brevibacterium* enzyme and the *Streptomyces* enzyme, the atomic temperature factors are comparable for both structures. In the *Streptomyces* structure, the glutamate oxygen atoms make hydrogen-bonding contacts with three water molecules in the active site (H_2O767, H_2O670, and H_2O541), all of which have clearly defined electron density (Figure 5a). A small extension of electron density is seen at OE1 of the glutamate side chain which may suggest some minor conformational flexibility of this side chain. However, it is not significant enough to model the side chain in a alternative conformation. The structure of the E361Q mutant adopts a main chain conformation identical to that of the native enzyme. The mutated glutamine side chain also adopts a conformation identical to that seen in the native structure with well-defined electron density. The identical hydrogen bonds are made between the side chain and the water molecules as is observed in the native structure. However, the bond to H_2O670 is considerably longer than that observed in the native structure (3.64 Å in the mutant as compared to 3.06 Å in the native structure). In addition, this side chain is involved in a fourth hydrogen-bonding contact to a water molecule (H_2O570) which is not present in the native structure. A careful analysis of the bound water molecules in the native structure shows H_2O1044 positioned 4.0 Å from OE1 of the glutamate side chain and 3.17 Å from O−Leu377. In the mutant, this water molecule is replaced by H_2O570 and H_2O902. H_2O902 is in hydrogen-bonding contact to N−Gln351, O−Phe359, and H_2O570. In addition to the hydrogen-bonding contact with H_2O902, H_2O570 makes a close contact to NE2−Gln361 and H_2O541 (Figure 5b).

In addition to the altered water structure in the direct vicinity of the glutamine side chain, H_2O672 is not present in the mutant structure. In the native structure this water molecule is positioned near the side chain of Val217 and makes extensive hydrogen-bonding contacts to five other water molecules in the substrate-binding pocket. In the mutant structure this water molecule is absent, resulting in the rearrangement of a number of distal water molecules at the top end of the substrate-binding pocket. However, the contacts near the isoalloxazine ring system and catalytic histidine residue (447) are structurally identical. Indeed, the position of the critical water molecule (H_2O541) differs by only 0.3 Å between the E361Q mutant and the native enzyme. Thus the mutation of the glutamate side chain results in a very slight arrangement of the water structure in the binding pocket of the enzyme, specifically in the more distal regions of the pocket.

Structure of His447Gln. Two mutants at position 447 were analyzed structurally. The native structure of cholesterol oxidase shows ND1 of His447 to be involved in a bifurcated hydrogen bond interaction with the side chain amides of Asn321 and Asn323. It is believed that this interaction is important in orienting the histidine ring in such a manner as to facilitate a hydrogen bond interaction between NE2 of the histidine ring and H_2O541. This water in turn makes a hydrogen bond interaction with N5 of the flavin cofactor. An analogous interaction has been reported in the structure of the *Brevibacterium* enzyme (*1*). Interestingly, in the H447Q mutant, the carbonyl of the amide group is involved in the identical bifurcated hydrogen bond interaction with the side chains of Asn321 and Asn323. However, superposition of the mutant and native structures shows that the side chain carbonyl oxygen of the glutamine (OE1) is positioned 1 Å from the ND1 position of the histidine ring in the native structure (Figure 6a). This results in a difference between NE2 of the histidine ring and NE2 of the glutamine side chain of 1.5 Å. To maintain the hydrogen-bonding network involving NE2−H447(Q447)/H_2O541/N5−FAD/OD1−N385/H2O670, the water molecule (H_2O541) shifts in the mutant structure by 1.1 Å from its position in the native structure. These shifts maintain the hydrogen bond between H_2O541 and Gln447 but also preserve the bonding network of interactions to other critical components of the active site.

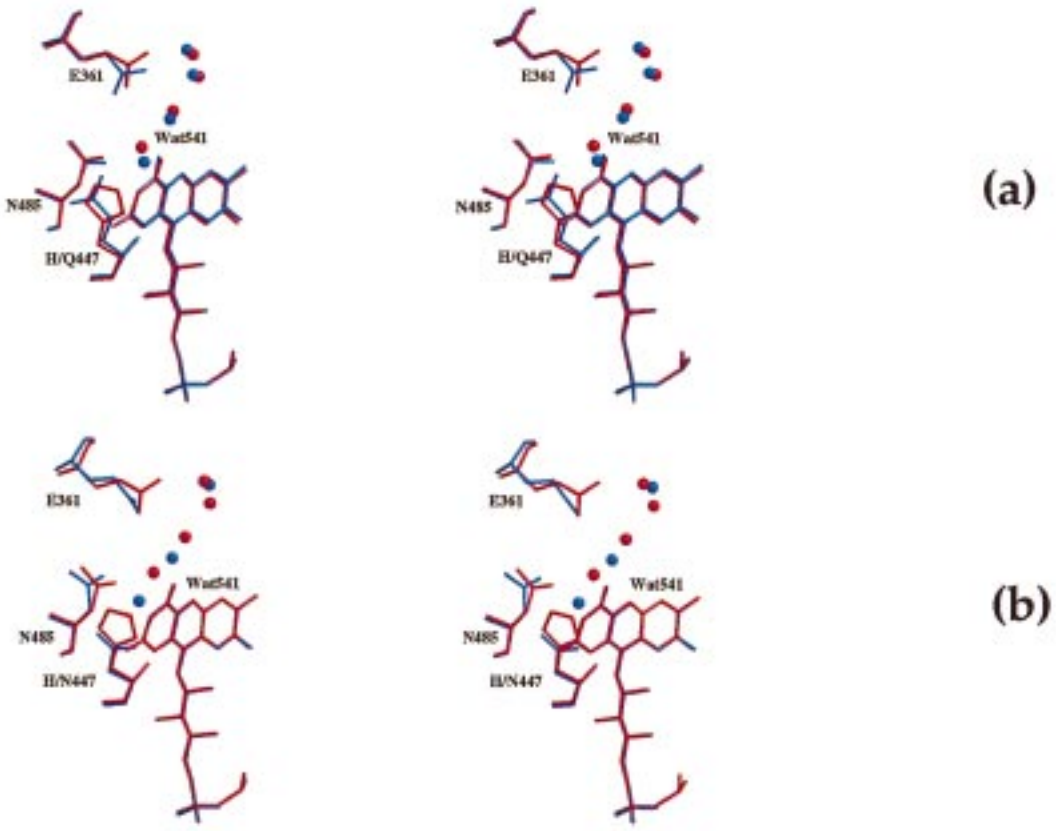

FIGURE 6: Stereo figures showing the superpositions of the native cholesterol oxidase from *Streptomyces* with (a) the His447Gln mutant and (b) the His447Asn mutant. The native structures are shown in blue, and the mutant structures are shown in red. Spheres represent water molecules located at or near the base of the substrate binding site.

Structure of His447Asn. The second mutation at position 447 was the introduction of an asparagine residue. This mutation resulted in a loss of the basic properties of the histidine side chain; however, some of the hydrogen-bonding properties were still maintained. Comparison of the structures of this mutant with the native enzyme shows that OD1 of the asparagine side chain superimposes with the position of ND1 of the histidine side chain. The bifurcated hydrogen bond interactions with Asn321 and Asn323 are still maintained in the mutant structure. However, the shortening of the side chain in the mutant results in a shift of the position of the second hydrogen-bonding atom, ND2. This atom is placed further back from the histidine NE2 position by 1.9 Å (Figure 6b). The shift of the ND2 atom results in a movement of the water molecule, H_2O541, by 1.8 Å. In addition, H_2O670 shifts by 1.5 Å in order to maintain the hydrogen bond with H_2O541. Further differences include a slight movement of Asn485 to accommodate the hydrogen bond to H_2O541. The movement of H_2O670 and H_2O541 results in a breakdown of the interactions with the rest of the water lattice in the active site cavity. There are significant shifts of the water molecules in the cavity as compared to the native structure.

Relationship of Mutant Activities to Their Structures. The catalytic activity of cholesterol oxidase may be measured using either cholesterol or cholest-5-en-3-one as a substrate. With cholest-5-en-3-one as a substrate, only the isomerization activity is measured. With cholesterol as a substrate, either the oxidation and isomerization activity may be measured or solely the oxidation activity. Which catalytic reactions are observed depends on the assay used (*15*). Using these three assays, the function of the His447 and Glu361 mutants could be determined. On the basis of the *Brevibacterium* structure, His447 was identified as the most likely residue that could act as a general base catalyst during oxidation and an electrophilic catalyst during isomerization. Mutation of His447 to glutamine had no effect on k_{cat} and K_m for isomerization (*15*). This was somewhat surprising as the pK_a of an amide hydrogen is approximately 10 orders of magnitude higher than an imidazolium hydrogen. The structure of the H447Q active site suggests that the NE2 of the glutamine is oriented toward H_2O541 and that this water can hydrogen bond to the carbonyl of the cholest-5-en-3-one intermediate. The electrophilicity of the amide hydrogen may be increased by the bifurcated hydrogen bond interaction of the glutamine OE1 with the side chains of Asn321 and Asn323.

A similar interaction is observed in the H447N mutant structure. However, the shortened side chain of asparagine compared to glutamine results in greater movement of H_2O541 from its position in the native structure. This shift suggests that the substrate will be displaced by greater than 1.5 Å from its optimal position relative to Glu361, the base that deprotonates the 4β-hydrogen. The H447N mutant shows primary deuterium kinetic isotope effects on both the deprotonation and protonation steps of isomerization. These isotope effects indicate that formation of the dienolic intermediate is rate-determining in the mutant reaction. This step is not rate-determining in the wild-type reaction. Taken together, the large shift in the water structure and observation

of kinetic isotope effects indicate that the catalytic efficiency of H447N isomerization is impaired because of mispositioning of the substrate relative to the glutamate base for isomerization.

In contrast to the wild-type activity of H447Q in isomerization, the k_{cat} for the mutant-catalyzed oxidation reaction is reduced 120-fold. The K_m only increases 2-fold. The structure of the mutant confirmed that the protein is folded properly and that the remaining active site residues have not moved. The reduced oxidation activity suggests that an imidazole general base is required for oxidation of the 3-hydroxyl to a ketone. However, mutation of the histidine does not abolish the catalytic activity, and it seemed likely that another residue could be helping to deprotonate O3. In the H447Q crystal structure, Glu361 is still hydrogen bonded to H_2O541. Thus, structurally, it appears that Glu361 can act as the general base for oxidation, at least in the mutant-catalyzed reaction.

This role is consistent with the oxidation activity of the E361Q mutant. This mutant no longer catalyzes isomerization because the carboxylate base that deprotonates the 4β-hydrogen has been changed to an amide. However, the mutant still catalyzes oxidation, although k_{cat} is 30-fold slower than for wild type. The K_m changes minimally. This reduction in oxidation rate suggests that Glu361 acts as a general base in the oxidation reaction via a hydrogen bond network through Asn485 and H_2O541.

SUMMARY

Comparison of the *Brevibacterium* and *Streptomyces* cholesterol oxidase structures has highlighted important structural differences that rationalize their different catalytic activities and substrate specificities. Two loops that appear to act as lids to the substrate-binding site are much less mobile, i.e., have lower temperature factors, in the native *Streptomyces* enzyme than in the *Brevibacterium* enzyme despite the fact that the average temperature factors for all the protein atoms are comparable in both structures. It seems reasonable that this increased rigidity reduces the entropy loss that occurs upon binding substrate. Consequently, the *Streptomyces* enzyme is a more efficient catalyst. The larger loop from residues 78−87 forms an α-helix in the *Streptomyces* cholesterol oxidase that determines the specificity of the oxidase for C17 substituents on the steroid substrate (*18*). In modifying loop residues to alter specificity, the design process must not introduce additional flexibility into the lid. This consideration is especially of importance in engineering the protein to be a better larvicide.

Our structural and kinetic data indicate that His447 and Glu361 act as general base catalysts in association with conserved water H_2O541 and Asn485. The position of this water appears to be important and orients active site residues as well as substrate for optimal catalysis. The His447, Glu361, H_2O541, and Asn485 hydrogen bond network is conserved among other oxidoreductases (*29*). However, these GMC oxidoreductases do not catalyze 1,3-allylic isomerizations, and they show no primary amino acid sequence homology to cholesterol oxidase (*30*). Cholesterol oxidase was included as a member of the family because its tertiary structure is similar to another family member, glucose oxidase (*31*). As more and more proteins are sequenced and structurally characterized before their functions are determined, it is important to catalog structural motifs that identify function. Observation of this catalytic tetrad in flavoproteins of unknown function may be diagnostic for enzymes that catalyze the oxidation of unactivated alcohols.

ACKNOWLEDGMENT

We thank N. Croteau for crystallization of the protein and M. Cygler for access to X-ray diffraction equipment.

REFERENCES

1. Vrielink, A., Lloyd, L. F., and Blow, D. M. (1991) *J. Mol. Biol. 219*, 533−554.
2. Li, J., Vrielink, A., Brick, P., and Blow, D. M. (1993) *Biochemistry 32*, 11507−11515.
3. Lange, Y. (1992) *J. Lipid Res. 33*, 315−321.
4. Purcell, J. P., Greenplate, J. T., Jennings, M. G., Tyerse, J. S., Pershing, J. C., Sims, S. R., Prinsen, M. J., Corbin, D. R., Tran, M., Sammons, R. D., and Stonard, R. J. (1993) *Biochem. Biophys. Res. Commun. 196*, 1406−1413.
5. Greenplate, J. R., Duck, N. B., Pershing, J. C., and Purcell, J. P. (1995) *Entomol. Exp. Appl. 74*, 253−258.
6. Corbin, D. R., Greenplate, J. T., and Purcell, J. P. (1998) *HortScience 33*, 614−617.
7. Ghoshroy, K. B., Zhu, W., and Sampson, N. S. (1997) *Biochemistry 36*, 6133−6140.
8. Uwajima, T., Yagi, H., Nakamurs, S., and Terada, O. (1973) *Agric. Biol. Chem. 37*, 2345−2350.
9. Tomioka, H., Kagawa, M., and Nakamura, S. (1976) *J. Biochem. 79*, 903−915.
10. Arima, K., Nagasawa, M., Bae, M., and Tamura, G. (1969) *Agric. Biol. Chem. 33*, 1636−1643.
11. Kerenyi, F., Szentirmai, A., and Natonek, M. (1975) *Acta Microbiol. Acad. Sci. Hung. 22*, 487−496.
12. Cheetham, P. S. J., Dunnill, P., and Lilly, M. D. (1982) *Biochem. J. 201*, 515−521.
13. Gadda, G., Wels, G., Pollegioni, L., Zucchelli, S., Ambrosius, D., Pilone, M. S., and Ghisla, S. (1997) *Eur. J. Biochem. 250*, 369−376.
14. Ohta, T., Fujishiro, K., Yamaguchi, K., Tamura, Y., Aisaka, K., Uwajima, T., and Hasegawa, M. (1991) *Gene 103*, 93−96.
15. Kass, I. J., and Sampson, N. S. (1998) *Biochemistry* (in press).
16. Sampson, N. S., and Kass, I. J. (1997) *J. Am. Chem. Soc. 119*, 855−862.
17. Sampson, N. S., and Chen, X. (1998) *Protein Expression Purif. 12*, 347−352.
18. Sampson, N. S., Kass, I. J., and Ghoshroy, K. B. (1998) *Biochemistry 37*, 5770−5778.
19. Stura, E., and Wilson, I. A. (1990) *Methods: A companion to methods in enzymology*, Vol. 1, pp 38−49, Academic Press, New York.
20. Otwinowski, Z. (1993) in *Data collection and Processing: Proceedings of the CCP4 Study Weekend* (Sawyer, L., Isaccs, N., and Bailey, S., Eds.) pp 56−62, SERC Daresbury Laboratory, Warrington, U.K.
21. Navaza, J. (1991) *Acta Crystallogr. A50*, 157−163.
22. Jones, T. A., Zou, J.-Y., Cowan, S. W., and Kjeldgaard, M. (1991) *Acta Crystallogr. A47*, 110−119.
23. Brünger, A. T., Kuriyan, J., and Karplus, M. (1987) *Science 235*, 458−460.
24. Ishizaki, R., Hirayama, N., Shinkawa, H., Nimi, O., and Murooka, Y. (1989) *J. Bacteriol. 171*, 596−601.
25. Carrière, F., Thirstrup, K., Hjorth, S., Ferrato, F., Nielsen, P. F., Withers-Martinez, C., Cambillau, C., Boel, E., Thim, L., and Verger, R. (1997) *Biochemistry 36*, 239−248.
26. Egloff, M.-P., Marguet, F., Buono, F., Berger, R., Cambillau, C., and Tilbeurgh, H. V. (1995) *Biochemistry 34*, 2751−2762.

27. Derewenda, U., Brzozowski, A. M., Lawson, D. M., and Derewenda, Z. S. (1992) *Biochemistry 31*, 1532−1541.
28. Cambillau, C., Longhi, S., Nicolas, A., and Chrislaine, M. (1996) *Curr. Opin. Struct. Biol. 6*, 449−455.
29. Kiess, M., Hecht, H.-J., and Kalisz, H. M. (1998) *Eur. J. Biochem. 252*, 90−99.
30. Cavener, D. (1992) *J. Mol. Biol. 223*, 811−814.
31. Hecht, H. J., Kalisz, H. M., Hendle, J., Schmid, R. D., and Schomburg, D. (1993) *J. Mol. Biol. 229*, 153−172.
32. Kraulis, P. J. (1991) *J. Appl. Crystallogr. 24*, 946−950.
33. Merritt, E. A., and Bacon, D. J. (1997) *Methods Enzymol. 277*, 505−525.

BI982497J